Malaria Parasite Detection in Peripheral Blood Images

F. Boray Tek[1] , Andrew G. Dempster[2] and Izzet Kale[1,3]
[1]University of Westminster, Dept. Electronic Systems,
Applied DSP & VLSI Research Group, London, UK
[2]University of New South Wales,
School of Surveying and Spatial Information Systems, Sydney, Australia
[3]Eastern Mediterranean University
Applied DSP & VLSI Research Centre, Dept. Eng, N. Cyprus
boraytek@yahoo.co.uk, a.dempster@unsw.edu.au, kalei@wmin.ac.uk

Abstract

This paper investigates the possibility of computerised diagnosis of malaria and describes a method to detect malaria parasites (*Plasmodium spp*) in images acquired from Giemsa-stained peripheral blood samples using conventional light microscopes. Prior to processing, the images are transformed to match a reference image colour characteristics. The parasite detector utilises a Bayesian pixel classifier to mark stained pixels. The class conditional probability density functions of the stained and the non-stained classes are estimated using the non-parametric histogram method. The stained pixels are further processed to extract features (histogram, Hu moments, relative shape measurements, colour auto-correlogram) for a parasite/non-parasite classifier. A distance weighted K-nearest neighbour classifier is trained with the extracted features and a detailed performance comparison is presented. Our method achieves 74% sensitivity, 98% specificity, 88% positive prediction, and 95% negative prediction values for the parasite detection.

1 Introduction

Malaria is a serious disease caused by a blood parasite named *Plasmodium spp*. The World Health Organization estimates 300-500 million malaria cases and more than 1 million deaths per year [10]. The definitive diagnosis of malaria infection is done by searching for parasites in blood slides (films) through a microscope. However, this is a routine and time consuming task. Besides a recent study on the field shows the agreement rates among the clinical experts for the diagnosis are surprisingly low [9]. Hence, it is very important to produce a common standard tool which is able to perform diagnosis with same ground criteria uniformly everywhere.

In peripheral blood sample visual detection and recognition of *Plasmodium spp* is possible and efficient via a chemical process called (*Giemsa*) staining. The staining process slightly colourises the red blood cells (RBCs) but highlights *Plasmodium spp* parasites, white blood cells (WBC), and platelets or artefacts. The detection of *Plasmodium spp*

BMVC 2006 doi:10.5244/C.20.36

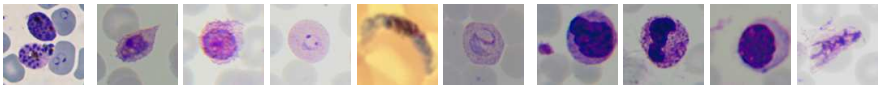

(a) (b) (c) (d) (e) (f) (g) (h) (i) (j)

Figure 1: Examples of stained objects: (a)-(f) Plasmodium, (g)-(i) WBCs (g) includes a platelet (j) artefact.

requires detection of the stained objects. However, to prevent false diagnosis the stained objects have to be analysed further to determine if they are parasites or not.

Automatic parasite detection has been addressed in [12], [13], [14] with thresholdings based on colour histograms. In [12], the image was pre-processed to remove the illumination bias which was estimated as the difference between the histogram peak positions of the colour channels (i.e. peak of blue - peak red/green). The markers for the parasites were extracted using a threshold at the halfway point of the cumulative histogram. However, in a diagnosis scenario, for every sample, such an approach would fail by marking all white blood cells (WBC), platelets and artefacts as parasites.

In this study we have proposed a solution for the parasite detection problem with two consecutive classifications: stained/non-stained pixel classification and parasite/non-parasite classification. Provided enough samples are present to estimate class conditional density functions, the Bayesian decision rule can be used as a powerful pixel classification method [3], [7], [8]. We have employed the Bayesian decision rule to determine if a pixel has stained or non-stained colour. The pixels that are classified as stained are further processed to form labelled connected components which are parasite candidates. Then these candidates are classified in a distance weighted K-nearest neighbour classifier to determine if they are parasites. For this classification, we have selected four different candidate features: colour histogram, Hu moments, shape measurements, and colour auto correlogram which are all rotation and scale invariant. We have evaluated and compared the performance of the individual selected features as well as their concatenated forms.

The organisation of the rest of the paper is as follows. Details of our method are discussed in Sections 2-4. The experimental results are provided in Section 5, and the conclusions are given in Section 6.

2 Colour Normalisation

It is essential to apply a colour normalisation to the images in order to decrease the effect of different light sources or sensor characteristics (e.g. intensity, white balance). Among many computational colour constancy algorithms [1] based on the different models of illumination change, we have chosen to use an adapted grey world normalisation method [17] based on the diagonal model of illumination change which utilises certain characteristics of microscopic peripheral blood images. Grey world normalisation assumes that there is a constant grey value of the image which does not change among different conditions. In the diagonal model an image of unknown illumination $\mathbf{I}^u$ can be simply transformed to known illuminant space $\tilde{\mathbf{I}^k}$ by multiplying pixel values with a diagonal matrix ($\mathbf{I}^{\tilde{k}}_{rgb}(x) = \mathbf{M}\mathbf{I}^u_{rgb}(x)$). Based on the grey world assumption, if there is an image with

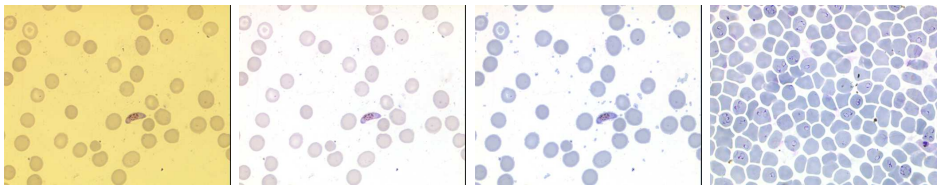

(a) (b) (c) (d)

Figure 2: Colour normalisation: (a) An input image before normalisation (b) after normalisation with its background channel average values, (c) (b) normalised with reference foreground channel averages, (d) a reference image.

known illuminant $\mathbf{I}^k$, the entries of the $\mathbf{M}$ can be calculated as follows:

$$\mathbf{M} = \begin{pmatrix} m_{11} & & \\ & m_{22} & \\ & & m_{33} \end{pmatrix} \quad m_{11} = \frac{\mu^{\mathbf{I}_r^k}}{\mu^{\mathbf{I}_r^u}} \quad m_{22} = \frac{\mu^{\mathbf{I}_g^k}}{\mu^{\mathbf{I}_g^u}} \quad m_{33} = \frac{\mu^{\mathbf{I}_b^k}}{\mu^{\mathbf{I}_b^u}} \tag{1}$$

where $\mu^{\mathbf{I}_{r,g,b}}$ are the means for channels r,g,b.

For ordinary images, a normalisation with a transformation using the average values yields poor results [1]. However, the images subject to this study contain two basic components (plasma and the rest) which can be separated by a foreground-background segmentation. Hence, the grey value assumption can be successfully incorporated into normalisation process [17]. In this method the input image is first separated into foreground and background regions. According to the method described in [12] which uses area morphology to estimate size of the cells and then extracts foreground objects and estimate histograms. After segmentation of the input, $\mathbf{I}^u_{r,g,b}$ channels foreground $(\mathbf{I}_{\mathbf{f}}{}^u_{r,g,b})$ and background $(\mathbf{I}_{\mathbf{b}}{}^u_{r,g,b})$ images are obtained and normalisation process can be described as follows:

1. Calculate $(\mathbf{I}_{\mathbf{b}}{}^u_{r,g,b})$ channel averages. Calculate $\mathbf{M^b}$: $m^b_{11,22,33} = \frac{1}{\mu^{\mathbf{I}_{\mathbf{b}}{}^u_{r,g,b}}}$.
2. Transform whole image: $I^1 = \mathbf{M^b}\, I^u$
3. Calculate $\mathbf{M^f}$: $m^f_{11,22,33}$ using equation (1) with $(\mathbf{I}_{\mathbf{f}}{}^1_{r,g,b})$ and the reference image foreground channels $\mathbf{I}_{\mathbf{f}}{}^c_{r,g,b}$).
4. Transform only the foreground channels: $\mathbf{I_f}^2 = \mathbf{M^f I_f}^1$
5. Replace the foreground channels of I^1 with $\mathbf{I_f}^2$.

The above procedure is quite efficient for the normalisation of the image with respect to global illumination and staining effects (under/over) according to a reference. The procedure is demonstrated with an example image in Figure 2.

3 Stained/Non-Stained Pixel Classification

Detection of the stained pixels can be viewed as a two class classification problem. Suppose the two classes are w_s for stained and w_{ns} for non-stained. A Bayesian classifier with

a feature in the form of $\mathbf{rgb} = \{r,g,b\}$ colour vector can be formulated as follows [3]:

$$\mathbf{rgb} \in w_s \qquad if \qquad \frac{p(\mathbf{rgb}|w_s)}{p(\mathbf{rgb}|w_{ns})} \geq \theta, \tag{2}$$

where $p(\mathbf{rgb}|w_i)$ ($i \in \{s,ns\}$) denotes the class conditional probability density function. θ can also be understood as a threshold for the likelihood ratio. It represents implicitly the application dependent costs for the decision and especially the *a priori* probabilities of classes $P(w_s)$, $P(w_{ns})$ when they are not easily determinable [3].

There are parametric, non-parametric and semi-parametric methods for estimating the $p(\mathbf{rgb}|w_i)$ [18]. In this study, we have used a non-parametric method based on histograms [7]. To calculate the probability density functions we have formed a training set of images in our image database. All the stained objects in the set were manually labelled *one by one* by thresholding with the help of a small program written for this task which facilitates viewing of the result of the image when adjusting two threshold values. Then the procedure for calculation of histograms is as described in [11]:

1. Initialise (to zero) 3-d histograms for both stained $H_s(r,g,b)$ and non-stained $H_{ns}(r,g,b)$ classes. Count every occurrence of (r,g,b) to construct the histograms:

$$\begin{array}{l} H_s(r,g,b) = H_s(r,g,b) + 1; \quad if \quad \mathbf{rgb} \in w_s \\ H_{ns}(r,g,b) = H_{ns}(r,g,b) + 1; \quad if \quad \mathbf{rgb} \in w_{ns} \end{array} \tag{3}$$

2. Normalise by the number of total occurrences (N_s, N_{ns}), respectively.

$$p(\mathbf{rgb}|w_s) = \frac{H_s(r,g,b)}{N_s} \quad p(\mathbf{rgb}|w_{ns}) = \frac{H_{ns}(r,g,b)}{N_{ns}} \tag{4}$$

In the images used in this study each channel is normally quantised to 256 levels. Building the 3-d histograms of H_s or H_{ns} with 256 levels in each channel requires 256^3 separate bins. This has two drawbacks; the first is that the required amount of samples for training (to estimate distributions) will be huge, a problem generally referred as the curse of dimensionality; the second but less important is the memory requirement. Hence, we ran our experiments on quantisation levels such as $16, 32, 64, 128$ and determined the optimal level according to the receiver operating characteristic (ROC) curves [18].

4 Parasite/Non-Parasite Classification

As mentioned earlier stained structures in blood slide images contain components other than the parasites such as WBCs, platelets or staining artefacts. In order to finalise the detection further classification is required.

Calculating area pattern spectrum function ($G_\Lambda(X)$) on the negative of the grey level image gives a good estimate for the average value of RBC area A_μ and radius [16]. A_μ is found by calculating the peak index of the $G_\Lambda(X)$: the differential plot of the reduced volume by successive area openings with an increasing area parameter. Let $\gamma^a_{\lambda_i}(X)$ denotes area opening of an image X with area threshold λ_i, then the calculation is as in (5).

$$G_\Lambda(X) = \sum \gamma^a_{\lambda_i}(X) - \sum \gamma^a_{\lambda_{i-1}}(X) \qquad \Lambda = \{\lambda_1, \lambda_2, ..., \lambda_n\} \tag{5}$$

After detecting the stained pixels, we apply infinite morphological reconstruction [15] using the stained pixel group S as markers and the negative grey level image to approximate the cell region which includes the stained group. The resulting binary region S_b is labelled for the feature extraction. Some stained pixel groups belonging to the same regions are merged by this process. Some of the non-parasites can be eliminated at this stage directly by comparing to the average cell size and location (background, foreground) by heuristics. For instance:

1. Eliminate stained group S if $Area(S) > k * A_\mu, \quad k > 1$
2. Eliminate stained group S if $Area(S) < m * A_\mu$ and $B_\mu(S) < t, \quad 0 < (t,k) < 1$

where the first rule checks for WBCs, which are bigger than the RBCs, and the second checks for the platelets which are (in most cases) smaller than RBCs and are almost surrounded by background. Note that these heuristics may only work with large WBCs and some artefacts and platelets which are clearly surrounded by background which is checked by calculating the foreground background pixel ratio $B_\mu(S)$ on the border of stained group S. However, in this study all the objects are passed to the feature extraction step and classified in the parasite/non-parasite classifier regardless of the heuristics.

4.1 Feature Extraction

Even for humans, parasite/non-parasite classification is not an easy task without special training. The parasite is a non-rigid object that can have a large variation in the observed morphology (Figure 1). The colour information is valuable but may not be adequate to distinguish the parasites from other stained objects. Raw images can not be used directly as features due to high variations in morphology which are coupled with arbitrary rotations and scales. A feature to be used in this classification must provide rotation, scale invariance and must be capable of capturing the morphological characteristics. We have chosen 4 different candidate features: (colour histogram, Hu moments, colour auto correlogram (henceforth correlogram), and a relative shape measurements vector) to investigate their individual performances and then search for a higher combined feature performance. The histogram is a widely used descriptor which is simple to compute and gives adequate information about the colour distribution. Hu's moment invariants are derived from algebraic combinations of the first 3 orders of normalised central moments. They are also rotation and scale invariant while providing spatial information [5]. The third feature, what we call the relative shape measurements vector, is formed of simple measurements to represent the object shape. The correlogram can be seen as an extended histogram: carries spatial information in addition to colour distribution. It has been proposed in [6] for image indexing and sub-region localisation and was used in [2] for object recognition.
Colour histogram $\mathbf{H}$ is the count of the occurrences of the colour c_i in image I:

$$H(c_i) \stackrel{\Delta}{=} \|I_{c_i}\| \qquad c_i \in C = \{c_1, c_2, \ldots, c_N\} \tag{6}$$

It can be normalised by the total number of pixels n to reflect the probability that a randomly chosen pixel will have the colour c_i. $h(c_i) = H(c_i)/n$.
Hu moments $\mathbf{M}$ is a 7 element feature vector which includes algebraic combinations of normalised central moments [5].

Relative shape measurements **R** is a 6 element vector containing the measurements below: Let S denote a stained object, S_b a foreground region (cell) in which S is contained, $a(S), p(S)$ are the area and the perimeter of S, $m(S)$ moment of inertia of S, A_μ average cell area in I. Then **R** can be expressed as:

$$\mathbf{R} \stackrel{\Delta}{=} \left\{ \frac{a(S)}{a(S_b)}, \frac{a(S)}{A_\mu}, \frac{a(S_b)}{A_\mu}, \frac{m(S)}{{A_\mu}^2}, \frac{4\,\pi\, a(S)}{p^2(S)}, \frac{4\,\pi\, a(S_b)}{p^2(S_b)} \right\} \tag{7}$$

Correlogram **C**: Suppose, the input image I is quantised to have N distinct colours ($c_i \in Q = \{c_1, c_2, \ldots, c_N\}$) and D denote a predetermined distance set ($k_i \in D = \{k_1, k_2, \ldots, k_M\}$). Then **C** is the count of co-occurrences of pixels p_1, p_2 of colour c_i which are k_i distance apart in I:

$$C(c_i, k_i) \stackrel{\Delta}{=} \| I(p_1) = c_i, |p_2 - p_1 = k | I(p_2) = c_i \| \tag{8}$$

It can be normalised to reflect the probability that a randomly chosen pixel will have colour c_i and co-occur with another c_i colour pixel in k distance by dividing to $(8k\, h(c_i))$ which is the total number of pixels in distance k times $h(c_i)$ the probability of observing colour c_i. The $8k$ is due to the distance calculation with the city block measure. For example, a centre pixel has 8 related pixels in distance $k = 1$, 16 related pixels in $k = 2$.

4.2 Classifier

To classify the stained objects we have implemented a distance weighted K-nearest neighbour classifier (Knn-d) [3], [4].
Knn-d: Assigns a query vector to the class $w_c \in W = \{w_1, \ldots, w_m\}$ which has the largest distance weighted majority (number/total distance) in the set of K closest (determined by a distance measure) neighbours in the training set.
Distance Measure: The choice of distance measure is critical for Knn classifiers. The possible choices for a simple measure can be the L_1 norm (D_{L1}), a relative distance measure based on L_1 norm [6] (D_{RL1}), or L_2 norm (D_{L2}).

$$D_{L1}(\mathbf{x}, \acute{\mathbf{x}}) \stackrel{\Delta}{=} \sum_{k=1}^{N} |x_k - \acute{x}_k|,\ D_{RL1}(\mathbf{x}, \acute{\mathbf{x}}) \stackrel{\Delta}{=} \sum_{k=1}^{N} \frac{|x_k - \acute{x}_k|}{1 + |x_k| + |\acute{x}_k|},\ D_{L2}(\mathbf{x}, \acute{\mathbf{x}}) \stackrel{\Delta}{=} \sqrt{\sum_{k=1}^{N} |x_k - \acute{x}_k|^2} \tag{9}$$

The D_{L2} (Euclidean distance) is known to be less robust against outliers than the D_{L1} (city block distance) [3]. We have chosen to use D_{RL1} which weights the contribution of each element to D_{L1} according to the magnitudes.
Classification Performance: Let $N_t^{w_1}$, $N_t^{w_2}$ show the number of test vectors in set Tt which are known to belong to the w_1 and w_2 classes, respectively. For a diagnosis problem like this, the analysis of four ratios can represent our method's performance. Let tp^{w_i}, fn^{w_i} show the number of correct and missed classifications for class w_i respectively.

$$SE = \frac{tp^{w_1}}{N_t^{w_1}}, \qquad SP = \frac{tp^{w_2}}{N_t^{w_2}}, \qquad PvP = \frac{tp^{w_1}}{tp^{w_1} + fn^{w_2}}, \qquad PvN = \frac{tp^{w_2}}{tp^{w_2} + fn^{w_1}} \tag{10}$$

where SE, SP, PvP, PvN denote sensitivity, specificity, prediction value positive, and prediction value negative respectively. The former two are usually named as the true detection rates for w_1 and w_2. Overall error can be summarised as $Err = \frac{nf^{w_1} + nf^{w_2}}{N_t}$.

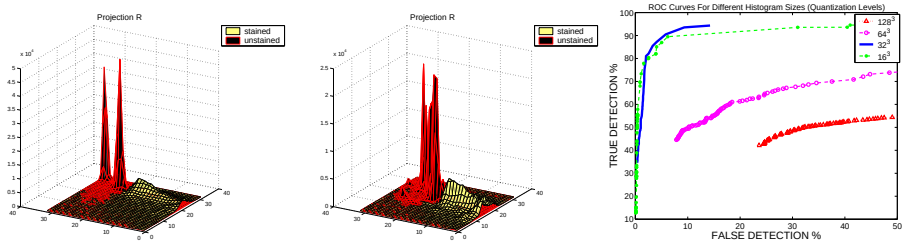

(a) (b) (c)

Figure 3: (a) Red axis projections of 3d histograms for stained (light-yellow) and non-stained (dark-red) classes, (b) Same plot in (a) using unnormalised images, (c) ROC curves for different histogram bin sizes.

5 Experiments and Results

Stained/Non-Stained Pixel Classification: We formed 3 separate sets for training (T_a), validation (T_θ), and testing (T_t) containing 286041 / 37050319, 205996 / 22705363, 168483 / 25209681 stained/non-stained pixels respectively. Since histograms are conditional density estimations we needed to find the appropriate histogram bin size which provides the maximum generalisation with finite samples. Additionally, we have to determine the threshold value θ for the histogram bin size which will be used in the classification. These two variables (bin size and threshold value) are usually determined by plotting receiver operating characteristics (ROC represents the trade-off between the true and false detection rates) on a validation test [18]. Then the variables that maximise the area under the ROC curve are chosen for the final tests. Figure 3(c) shows different ROC curves (in T_θ) of different sizes of histograms (quantisation levels :$128, 64, 32, 16$). Examining these ROC curves, it is apparent that the most efficient histogram bin size is 32 with the largest rate of true detection and the lowest rate of false detection. For the 32 histogram bin size, threshold value $\theta = 2.6$ provides the best rates and was used for testing the test set T_t. Based on this observation we set the bin sizes to 32^3 for the histograms and calculated the performance. In order to observe the distribution of the two classes and observe the colour normalisation effect (projections on the red axis) cumulative histograms are plotted in Figure 3 which are projections of the actual histograms that are in 3-d (r,g,b). The test set performance for $\theta = 2.6$ is shown in Table 1 together with the results of the threshold method described in [12]. The results show that the Bayesian classifier outperforms the threshold method. Also, the colour normalisation improves the overall procedure of Bayesian stained/non-stained pixel classification (Table 1). However, for the threshold method we were not able to see the normalisation effect since it assumes the peak of the blue channel minus the peak of the max(red/green) channel gives the illumination bias which does not hold after normalisation.

Parasite/Non-Parasite Stained Object Classification: Due to the low number of parasites versus non-parasites in total of 260 images, we have formed 2 separate sets of stained objects for training (T_a), and testing (T_t) containing $175/1312$, $202/1311$, parasite/non-parasite objects respectively. In T_a, the RGB images were indexed with minimum variance quantisation to have 32 distinct colours, the same indexed colour map is applied to the images in T_t. In the correlogram calculations the distance set was $D = \{1, 2, \ldots, 8\}$ which

Method	# S.Pixels	T. D.%	F. D.%
Bayesian+Norm	168483	88.5	5.6
Bayesian	168483	84.5	17
Threshold [12]	168483	74	34

Table 1: Results of the pixel classifier on the test set T_t (68 images). T.D: true detection, F.D: false detection

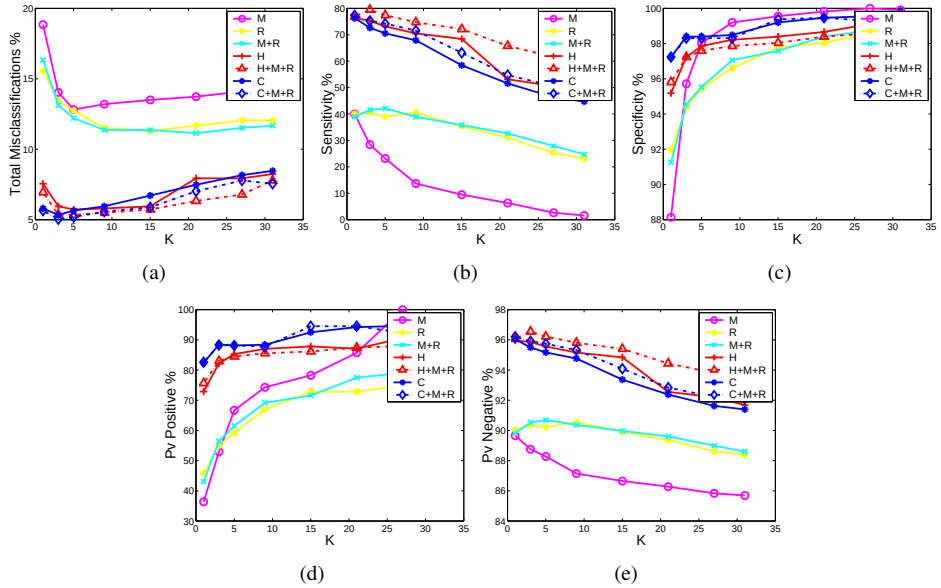

Figure 4: Percentages plotted against K: (a) Total misclassification, (b) *SE* sensitivity, (c) *SP* specificity, (d) *PvP* predictive value of parasites, (e) *PvN* predictive value of non-parasites. Features H:histogram, M:Hu moments, R:Relative shape measurements, C: Correlogram. (+) denotes concatenation.

results in $32x8$ dimensional feature vector. The average cell area A_μ was calculated for every image. All the features were normalised to have zero mean and unit variance.

Figure 4 shows the total misclassification percentage together with *SE*, *SP*, *PvP*, and *PvN* measurements plotted against increasing K in Knn-d classifier. The results are a validation of the overall process and performance comparison of the different features. An examination of the total classification error (Figure 4(a)) indicates the most successful feature is $C+M+R$ followed in the order by $H+M+R$, C, and H. Thus, feature C is more successful than H. However, the difference is not significant especially considering the cost in calculation time for C. The performances of M and R are low which suggests that colour information is essential. However, they provide slight boosts for the H and C features. To interpret the results in more detail, if we choose the value $K = 3$ in the feature $(C+M+R)$, the *SE* (74%) performance value reveals the probability of the result being positive given that the stained object is a parasite. The *SP* (98%) value reveals that the probability of the result being negative given that the object is not a parasite. The

PvP (88%) value reveals that the probability of the stained object being a parasite given a positive result. The PvN value shows that the negative case (of PvP) is 95%.

In addition to the above results, the performance of the heuristic elimination rules was separately evaluated to provide a comparison. On T_t (same as above) using the area rules (described in Section 2.3) 261 of 1109 non-parasites could be eliminated. By taking this as the number of correct classifications of non-parasites (the rest are assigned to parasite class) the performance measurements would be $SE = 100\%, SP = 23\%, PvP = 19\%, PvN = 100\%$. If the same tests were performed in the other studies which proposed stained object detection as the parasite detection mechanism [12], [13], [14] the performance values would be $SE = 100\%, SP = 0\%, PvP = 15\%, PvN = 0\%$.

6 Conclusion and Discussion

We have described a method that detects malaria parasites in images acquired from peripheral Giemsa-stained blood samples using conventional light microscopes. We have utilised a colour normalisation method to maintain illumination and colour constancy. We have demonstrated a solution for the stain extraction problem with a two class (stained/ non-stained) Bayesian classification. The results show that the stained pixel classifier achieves satisfactory results: 88.5%, 5.6% true and false detection rates respectively. The detected stained pixels are further processed to extract features H (histogram), M (Hu moments), R (relative shape measurements), C (colour auto correlogram) which are used in the parasite/non-parasite classifier. A Knn-d classifier has been implemented and detailed evaluations demonstrate the individual and concatenated feature performances. The colour based features: C and H were the most successful single features. The feature C was more successful than the feature H. However, the difference was not significant which may be caused by the high dimensionality of the feature C. The shape features: M and R alone did not have a significant outcome. Concatenations of $M+R$ were slightly boosting the C and H features. The evaluations here do not suggest concatenated features necessarily yield better results. Instead, they suggest colour based features are more successful in discriminating the parasites and non-parasites; and that adding shape based features to them slightly improves the performance.

We have shown that the stained pixel detection or stained object extraction as proposed in [12], [13], [14] does not lead to successful parasite detection; parasite detection can also not be performed with heuristics based only on area measurements. Our parasite/non-parasite classifier achieves 74% sensitivity, 98% specificity, 88% positive prediction, 95% negative prediction value rates based on a single observation. However, in a real diagnosis scenario a blood film from a test case could provide thousands of stained objects. Thus, the diagnostic decision can be made according to the decisions on the total number instead of a single one. To improve the efficiency of the method as a viable malaria diagnosis tool and to reveal the actual diagnosis performance more controlled experiments should be performed and compared to expert manual diagnosis.

References

[1] K. Barnard. *Practical colour constancy*. Ph.d. thesis, Simon Fraser University School of Computing Science, 1999.

[2] P. Chang and J. Krumm. Object recognition with color cooccurance histograms. In *Proc. IEEE Conf. on Computer Vision and Pattern Recognition*, June 1999.

[3] R. O. Duda, P. E. Hart, and D. G. Stork. *Pattern Classification*. Wiley-Interscience Publication, New York, 2000.

[4] S. Dudani. The distance-weighted k-nearest-neighbor rule. *IEEE Trans. on Systems, Man and Cybernetics*, 6:325–327, 1976.

[5] M-K. Hu. Visual pattern recognition by moment invariants. *IRE Trans. on Information Theory*, 8:179–187, 1962.

[6] J. Huang, S. R. Kumar, M. Mitra, W-J. Zhu, and R. Zabih. Spatial color indexing and applications. *Int. Journal of Computer Vision*, 35(3):245–268, 1999.

[7] M. J. Jones and J. M. Rehg. Statistical color models with application to skin detection. *Int. J. Comput. Vision*, 46(1):81–96, 2002.

[8] O. Lezoray and H. Cardot. Bayesian marker extraction for color watershed in segmenting microscopic images. In *Proc. Pattern Recognition*, volume 1, pages 739–742, 2002.

[9] K. Mitiku, G. Mengistu, and B. Gelaw. The reliability of blood film examination for malaria at the peripheral health unit. *Ethiop.J.Health Dev*, 17(3):197–204, 2003.

[10] World Health Organization. What is malaria? fact sheet no94. *http://www.who.int/mediacentre/factsheets/fs094/en/*.

[11] S. L. Phung, A. Bouzerdoum, and D. Chai. Skin segmentation using color pixel classification: analysis and comparison. *IEEE Transactions on Pattern Analysis and Machine Intelligence*, 27(1):148–154, 2005.

[12] KNR. M. Rao. *Application of Mathematical Morphology to Biomedical Image Processing*. PhD thesis, U. Westminster, 2004.

[13] C. Di Ruberto, A. Dempster, S. Khan, and B. Jarra. Automatic thresholding of infected blood images using granulometry and regional extrema. In *ICPR*, pages 3445–3448, 2000.

[14] C. Di Ruberto, A. Dempster, S. Khan, and B. Jarra. Analysis of infected blood cell images using morphological operators. *IVC*, 20(2):133–146, February 2002.

[15] P. Soille. *Morphological Image Analysis*. Springer-Verlag, Heidelberg, 2003.

[16] F. B. Tek, A. G. Dempster, and I. Kale. Blood cell segmentation using minimum area watershed and circle radon transformations. In *Proc. Int. Symp. on Mathematical Morphology*, volume 1, pages 739–752, April 2005.

[17] F. B. Tek, A. G. Dempster, and I. Kale. A colour normalization method for giemsa-stained blood cell images. In *Proc. Sinyal Isleme ve Iletisim Uygulamalari*, April 2006.

[18] A. Webb. *Statistical pattern recognition 2nd Ed.* J Wiley and Sons Inc., New York, USA, 2002.